Kinetostatic Performance of a Planar Parallel Mechanism with Variable Actuation

Novona Rakotomanga, Damien Chablat, Stéphane Caro

Kinetostatic Performance of a Planar Parallel Mechanism with Variable Actuation

N. Rakotomanga, D. Chablat and S. Caro

[1]*École de Technologie Supérieure, Montréal, QC, Canada,*
e-mail: novona.rakotomanga.1@ens.etsmtl.ca
[2]*Institut de Recherche en Communications et Cybernétique de Nantes, France,*
e-mail: {damien.chablat, stephane.caro}@irccyn.ec-nantes.fr

Abstract. This paper deals with a new planar parallel mechanism with variable actuation and its kinetostatic performance. A drawback of parallel mechanisms is the non homogeneity of kinetostatic performance within their workspace. The common approach to solve this problem is the introduction of actuation redundancy, that involves force control algorithms. Another approach, highlighted in this paper, is to select the actuated joint in each limb with regard to the pose of the end-effector. First, the architecture of the mechanism and two kinetostatic performance indices are described. Then, the actuating modes of the mechanism are compared.

Key words: Parallel mechanism, regular dextrous workspace, variable actuated mechanism.

1 Introduction

A drawback of serial and parallel mechanisms is the inhomogeneity of the kinetostatic performance within their workspace. For instance, dexterity, accuracy and stiffness are usually bad in the neighbourhood of singularities that can appear in the workspace of such mechanisms. As far as the parallel mechanisms are concerned, their inverse kinematics problem (IKP) has usually many solutions, which correspond to the *working modes* of the mechanism [4]. Nevertheless, it is difficult to come up with a large workspace free of singularity with a given working mode. Consequently, a trajectory planning may require a change of the working mode by means of an alternative trajectory in order to avoid singular configurations. In such a case, the initial trajectory would not be followed. The common approach to solve this problem is to introduce actuation redundancy, that involves force control algorithms [1]. Another approach is to use the concept of joint-coupling as proposed by [15] or to select the actuated joint in each limb with regard to the pose of the end-effector, [2], as highlighted in this paper. Therefore, we introduce a planar parallel mechanism with variable actuation, also known as *variable actuated mechanism* (VAM). First, the architecture of the mechanism and two kinetostatic performance indices are described. Then, the *actuating modes* (AMs) of the mechanism are compared based on their kinetostatic performance.

2 Preliminaries

This section deals with the kinematic modeling of a new variable actuated mechanism (VAM), its singularity analysis, the presentation of some performance indices and the concept of regular dextrous workspace.

2.1 Mechanism architecture

The concept of VAM was introduced in [2, 15]. Indeed, they derived a VAM from the architecture of the 3-RPR planar parallel manipulator (PPM) by actuating either the first revolute joint or the prismatic joint of its limbs. This paper deals with the
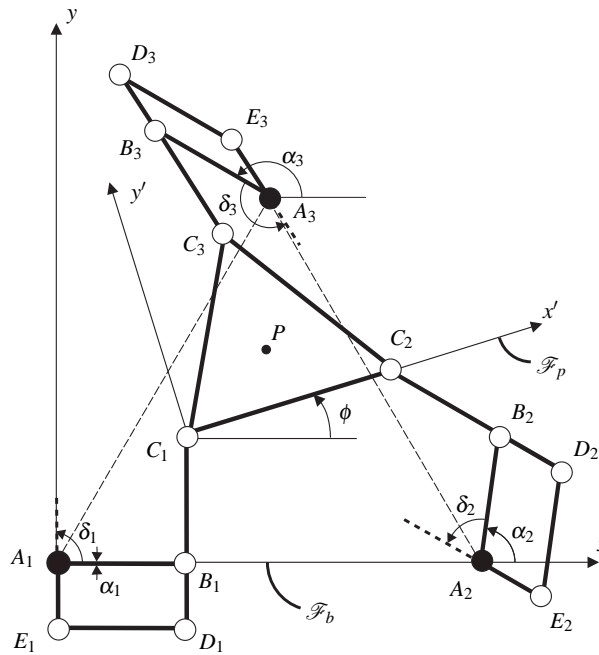
Fig. 1 3-RRR PPM with variable actuation

study of a new VAM illustrated in Figure 1. This mechanism is derived from the architecture of the 3-RRR PPM. As a matter of fact, the first link of each limb of the conventional 3-RRR manipulator is replaced by parallelogram $A_iB_iD_iE_i$ to come up with the mechanism at hand. Accordingly, links A_iB_i and B_iC_i can be driven independently, i.e., angles α_i and δ_i are actuated and uncoupled, by means of an actuator and a double clutch mounted to the base and located in point A_i, $i = 1, 2, 3$.

It turns out that the VAM has eight *actuating modes* as shown in Table 1. Indeed, the actuating mode of the mechanism depends on its actuated joints. For instance, the first actuating mode corresponds to the 3-RRR mechanism, also called $\underline{R}RR_1$-$\underline{R}RR_2$-$\underline{R}RR_3$ mechanism in the scope of this paper, as the first revolute joints (located in point A_i) of its limbs are actuated. Likewise, the eighth actuating mode corresponds to the 3-RRR manipulator, also called $R\underline{R}R_1$-$R\underline{R}R_2$-$R\underline{R}R_3$ mechanism, as the second revolute joints (located in point B_i) of its limbs are actuated.

The moving platform pose of the VAM is determined by means of the Cartesian coordinates (x,y) of operation point P expressed in frame $\mathscr{F}_b$ and angle ϕ, namely, the angle between frames $\mathscr{F}_b$ and $\mathscr{F}_p$. Moreover, the passive and actuated joints do not have any stop. Points A_1, A_2 and A_3, (C_1, C_2 and C_3, respectively) lie at the corners of an equilateral triangle, of which the geometric center is point O (point P, resp.). The length of links A_iB_i and B_iC_i is equal to 3.0, $i = 1,2,3$. The length of segment A_1A_2 (C_1C_2, resp.) is equal to 10.0 (5.0, resp.). The unit is not specified as absolute lengths are not necessary to convey the idea.

Table 1 The eight actuating modes of the 3-RRR VAM

Actuating mode number	driven links	active angles
1	$\underline{R}RR_1$-$\underline{R}RR_2$-$\underline{R}RR_3$	A_1B_1, A_2B_2, A_3B_3	$\alpha_1, \alpha_2, \alpha_3$
2	$\underline{R}RR_1$-$\underline{R}RR_2$-$R\underline{R}R_3$	A_1B_1, A_2B_2, A_3E_3	$\alpha_1, \alpha_2, \delta_3$
3	$\underline{R}RR_1$-$R\underline{R}R_2$-$\underline{R}RR_3$	A_1B_1, A_2E_2, A_3B_3	$\alpha_1, \delta_2, \alpha_3$
4	$R\underline{R}R_1$-$\underline{R}RR_2$-$\underline{R}RR_3$	A_1E_1, A_2B_2, A_3B_3	$\delta_1, \alpha_2, \alpha_3$
5	$\underline{R}RR_1$-$R\underline{R}R_2$-$R\underline{R}R_3$	A_1B_1, A_2E_2, A_3E_3	$\alpha_1, \delta_2, \delta_3$
6	$R\underline{R}R_1$-$R\underline{R}R_2$-$\underline{R}RR_3$	A_1E_1, A_2E_2, A_3B_3	$\delta_1, \delta_2, \alpha_3$
7	$R\underline{R}R_1$-$\underline{R}RR_2$-$R\underline{R}R_3$	A_1E_1, A_2B_2, A_3E_3	$\delta_1, \alpha_2, \delta_3$
8	$R\underline{R}R_1$-$R\underline{R}R_2$-$R\underline{R}R_3$	A_1E_1, A_2E_2, A_3E_3	$\delta_1, \delta_2, \delta_3$

2.2 Kinematic modeling

The velocity $\dot{\mathbf{p}}$ of point P can be obtained in three different forms, depending on which leg is traversed, namely,

$$\dot{\mathbf{p}} = \dot{\alpha}_1\mathbf{E}(\mathbf{c}_1 - \mathbf{a}_1) + \dot{\delta}_1\mathbf{E}(\mathbf{c}_1 - \mathbf{b}_1) + \dot{\phi}\mathbf{E}(\mathbf{p} - \mathbf{c}_1) \tag{1}$$

$$\dot{\mathbf{p}} = \dot{\alpha}_2\mathbf{E}(\mathbf{c}_2 - \mathbf{a}_2) + \dot{\delta}_2\mathbf{E}(\mathbf{c}_2 - \mathbf{b}_2) + \dot{\phi}\mathbf{E}(\mathbf{p} - \mathbf{c}_2) \tag{2}$$

$$\dot{\mathbf{p}} = \dot{\alpha}_3\mathbf{E}(\mathbf{c}_3 - \mathbf{a}_3) + \dot{\delta}_3\mathbf{E}(\mathbf{c}_3 - \mathbf{b}_3) + \dot{\phi}\mathbf{E}(\mathbf{p} - \mathbf{c}_3) \tag{3}$$

with matrix $\mathbf{E}$ defined as

$$\mathbf{E} = \begin{bmatrix} 0 & -1 \\ 1 & 0 \end{bmatrix}$$

$\mathbf{a}_i$, $\mathbf{b}_i$ and $\mathbf{c}_i$ are the position vectors of points A_i, B_i and C_i, respectively. $\dot{\alpha}_i$, $\dot{\delta}_i$ and $\dot{\phi}$ are the rates of angles α_i, δ_i and ϕ depicted in Fig. 1, $i = 1, 2, 3$.

The kinematic model of the VAM under study can be obtained from Eqs.(1)-(c) by eliminating the idle joint rates. However, the latter depend on the actuating mode of the mechanism. For instance, $\dot{\delta}_1$, $\dot{\delta}_2$ and $\dot{\delta}_3$ are idle with the first actuating mode and the corresponding kinematic model is obtained by dot-multiplying Eqs.(1)-(c) with $(\mathbf{c}_i - \mathbf{b}_i)^T$, $i = 1, 2, 3$. Likewise, $\dot{\delta}_1$, $\dot{\delta}_2$ and $\dot{\alpha}_3$ are idle with the second actu-ating mode and the corresponding kinematic model is obtained by dot-multiplying Eqs.(1)-(b) with $(\mathbf{c}_i - \mathbf{b}_i)^T$, $i = 1, 2$, and Eq.(3) with $(\mathbf{c}_3 - \mathbf{a}_3)^T$.

The kinematic model of the VAM can now be cast in vector form, namely,

$$\mathbf{At} = \mathbf{B\dot{q}} \quad \text{with} \quad \mathbf{t} = [\dot{\mathbf{p}} \; \dot{\phi}]^T \quad \text{and} \quad \dot{\mathbf{q}} = [\dot{q}_1 \; \dot{q}_2 \; \dot{q}_3]^T \tag{4}$$

with $\dot{\mathbf{q}}$ thus being the vector of actuated joint rates. $\dot{q}_i = \dot{\alpha}_i$ when link A_iB_i is driven and $\dot{q}_i = \dot{\delta}_i$ when link A_iE_i is driven, $i = 1, 2, 3$. $\mathbf{A}$ and $\mathbf{B}$ are respectively, the direct and the inverse Jacobian matrices of the mechanism, defined as

$$\mathbf{A} = \begin{bmatrix} (\mathbf{c}_1 - \mathbf{h}_1)^T & -(\mathbf{c}_1 - \mathbf{h}_1)^T \mathbf{E}(\mathbf{p} - \mathbf{c}_1) \\ (\mathbf{c}_2 - \mathbf{h}_2)^T & -(\mathbf{c}_2 - \mathbf{h}_2)^T \mathbf{E}(\mathbf{p} - \mathbf{c}_2) \\ (\mathbf{c}_3 - \mathbf{h}_3)^T & -(\mathbf{c}_3 - \mathbf{h}_3)^T \mathbf{E}(\mathbf{p} - \mathbf{c}_3) \end{bmatrix} \tag{5}$$

$$\mathbf{B} = \text{diag} \left[(\mathbf{c}_i - \mathbf{b}_i)^T \mathbf{E}(\mathbf{b}_i - \mathbf{a}_i) \right], \quad i = 1, 2, 3 \tag{6}$$

where $\mathbf{h}_i = \mathbf{b}_i$ when link A_iB_i is driven and $\mathbf{h}_i = \mathbf{a}_i$ when link B_iC_i is driven, $i = 1, 2, 3$.

When $\mathbf{A}$ is non singular, we obtain the relation

$$\mathbf{t} = \mathbf{J\dot{q}} \quad \text{with} \quad \mathbf{J} = \mathbf{A}^{-1}\mathbf{B} \tag{7}$$

Likewise, we obtain

$$\dot{\mathbf{q}} = \mathbf{Kt} \tag{8}$$

when $\mathbf{B}$ is non singular with $\mathbf{K}$ denoting the inverse of $\mathbf{J}$.

2.3 Singularity analysis

The singular configurations associated with the direct-kinematic matrix of PPMs are well known [12]. For the 3-$\underline{R}$RR PPM, such configurations are reached whenever lines (B_1C_1), (B_2C_2) and (B_3C_3) intersect (possibly at infinity). For the 3-R$\underline{R}$R PPM, such configurations are reached whenever lines (A_1C_1), (A_2C_2) and (A_3C_3) inter-sect. Consequently, the singular configurations associated with the direct-kinematic matrix of the VAM are reached whenever lines (H_1C_1), (H_2C_2) and (H_3C_3) intersect where H_i stands for B_i (A_i, resp.) when link A_iB_i (B_iC_i, resp.) is driven, $i = 1, 2, 3$.

From Eq.(6), the singular configurations associated with the inverse-kinematics of the VAM are reached whenever points A_i, B_i, and C_i are aligned.

2.4 Performance indices

We focus here on issues pertaining to manipulability or dexterity. In this regard, we understand these terms in the sense of measures of distance to singularity, which brings us to the concept of condition number in [9]. Here, we adopt the *condition number* of the underlying Jacobian matrices based on the Frobenius norm as a means to quantify distances to singularity and the *transmission angle*.

2.4.1 Condition number

The *condition number* $\kappa_F(\mathbf{M})$ of a $m \times n$ matrix $\mathbf{M}$, with $m \leq n$, based on the Frobenius norm is defined as follows

$$\kappa_F(\mathbf{M}) = \frac{1}{m} \sqrt{\text{tr}(\mathbf{M}^T\mathbf{M})\text{tr}\left[(\mathbf{M}^T\mathbf{M})^{-1}\right]} \tag{9}$$

Here, the condition number is computed based on the Frobenius norm as the latter produces a condition number that is analytic in terms of the posture parameters whereas the 2-norm does not. Besides, it is much costlier to compute singular values than to compute matrix inverses.

   The terms of the direct Jacobian matrix of the VAM are not homogeneous as they do not have same units. Accordingly, its condition number is meaningless. Indeed, its singular values cannot be arranged in order as they are of different nature. However, from [11] and [13], the Jacobian can be normalized by means of a *normalizing length*. Later on, the concept of *characteristic length* was introduced in [14] in order to avoid the random choice of the normalizing length. For instance, the previous concept was used in [5] to analyze the kinetostatic performance of manipulators with multiple inverse kinematic solutions, and therefore to select their best *working mode*.

2.4.2 Transmission angle

The *transmission angle* can be used to assess the quality of force transmission in mechanisms involving passive joints. Although it is well known and easily computable for 1-DOF or single loop mechanisms [3, 8], it is not extensively used for n-DOF mechanical systems ($n > 1$) [2].

   The transmission angle ψ_i is defined as an angle between vectors of force $\mathbf{Fc}_i$ and translational velocity $\mathbf{Vc}_i$ of a point to which the force is applied as illustrated in Fig. 2. When link A_iB_i is driven, the direction of force $\mathbf{Fc}_i$ is the direction of link B_iC_i, namely,

$$\gamma_i = \arctan\left(\frac{y_{C_i} - y_{B_i}}{x_{C_i} - x_{B_i}}\right), i = 1,2,3 \tag{10}$$
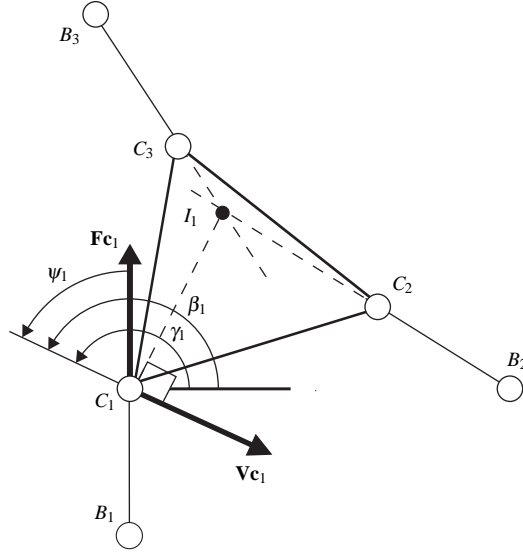
Fig. 2 Transmission angle of the 3-<u>R</u>RR manipulator

Conversely, when link $A_i E_i$ is driven, the direction of force $\mathbf{Fc}_i$ is the direction of line $(A_i C_i)$, namely,

$$\gamma_i = \arctan\left(\frac{y_{C_i} - y_{A_i}}{x_{C_i} - x_{A_i}}\right), i = 1, 2, 3 \tag{11}$$

The instantaneous centre of rotation depends on the leg under study. For example, instantaneous centre of rotation I_1 associated with leg 1 is the intersecting point of forces $\mathbf{Fc}_2$ anf $\mathbf{Fc}_3$. Table 2 gives the Cartesian coordinates of instantaneous centre

Table 2 Cartesian coordinates of instantaneous centres of rotation

	I_1	I_2	I_3
x_{I_i}	$\dfrac{b_3 - b_2}{\tan(\gamma_2) - \tan(\gamma_3)}$	$\dfrac{b_1 - b_3}{\tan(\gamma_3) - \tan(\gamma_1)}$	$\dfrac{b_2 - b_1}{\tan(\gamma_1) - \tan(\gamma_2)}$
y_{I_i}	$\dfrac{b_3 \tan(\gamma_2) - b_2 \tan(\gamma_3)}{\tan(\gamma_2) - \tan(\gamma_3)}$	$\dfrac{b_1 \tan(\gamma_3) - b_3 \tan(\gamma_1)}{\tan(\gamma_3) - \tan(\gamma_1)}$	$\dfrac{b_2 \tan(\gamma_1) - b_1 \tan(\gamma_2)}{\tan(\gamma_1) - \tan(\gamma_2)}$

of rotation I_i associated with the ith leg of the VAM, expressed in frame $\mathscr{F}_b$, with $b_i = y_{C_i} - x_{C_i} \tan \gamma_i$, $i = 1, 2, 3$. The direction of $\mathbf{Vc}_i$ is defined as,

$$\beta_i = \arctan\left(\frac{y_{C_i} - y_{I_i}}{x_{C_i} - x_{I_i}}\right) + \frac{\pi}{2}, i = 1, 2, 3 \tag{12}$$

The transmission angle related to the ith leg of the VAM is defined as follows,

$$\psi_i = |\gamma_i - \beta_i|, \, i = 1, 2, 3 \tag{13}$$

and the transmission angle ψ of the mechanism is defined as,

$$\psi = \max(\psi_i), \, i = 1, 2, 3 \tag{14}$$

Finally, the smaller ψ, the better the force transmission of the mechanism.

2.4.3 Regular dextrous workspace

A manipulator had better keep good and homogeneous performance within its workspace. For that reason, the concept of *regular dextrous workspace* is introduced in [6]. In fact, the regular dextrous workspace of a manipulator is a regular-shaped workspace included in its Cartesian workspace with good and homogeneous performance. As we focus on the kinetostatic performance of the VAM in the scope of this paper, we consider only the condition number of its kinematic Jacobian matrix and its transmission angle as performance indices.

3 Actuating Modes Comparison

For the VAM under study, the inverse condition number of its kinematic Jacobian matrix, i.e., $\kappa_F^{-1}(\mathbf{J})$ with $\mathbf{J}$ defined in Eq.(7), varies from 0 to 1 within its workspace $\mathscr{W}$. Likewise, its transmission angle ψ, defined in Eq.(14), varies from 0 to $90°$ within $\mathscr{W}$. From [2], a mechanism has good kinetostatic performance as long as its transmission angle is smaller than $75°$. Let us assume that the kinetostatic performance are good as well as long as $\kappa_F^{-1}(\mathbf{J}) > 0.15$. Therefore, we claim that the VAM and its actuating modes (AMs) have good kinetostatic performance as long as $\kappa_F^{-1}(\mathbf{J})$ is higher than 0.15 and ψ is smaller than $75°$.

First, let us compare the size of the workspace corresponding to AMs of the VAM given in Table 1, based on the two previous kinetostatic performance indices. In this vein, let us consider that the orientation, ϕ, of the moving platform of the VAM is constant and the latter stays as far as possible from singular configurations, i.e., let ϕ be equal to $17.5°$. From Table 3, we can notice that the size of the workspace corresponding to the 2nd, 3rd and 4th AMs is the same. Likewise, the size of the workspace corresponding to the 4th, 5th and 6th AMs is the same. This is due to the symmetric architecture of the mechanism. Moreover, the largest workspace is obtained with the 1st AM and the smallest one with the 8th AM. Finally, we can notice that the two kinematic performance indices give similar results.

In order to compare the AMs of the VAM, we also assume that its regular dextrous workspace (RDW) is a cylinder, of which the section depicts the position (x, y) of its moving platform and the height shows the rotation ϕ of the latter. Let ϕ vary between $5°$ and $25°$. Figures 3(a)-(e) (Figures 4(a)-(e), resp.) illustrate the kineto-

Table 3 Ratio of the VAM actuating modes workspace size to the VAM workspace size with $\kappa_F^{-1}(\mathbf{J}) > 0.15$ and $\psi < 75°$, $\phi = 17.5°$

| Actuating mode	Workspace size ratio [%]	
number	$\kappa_F^{-1}(\mathbf{J}) > 0.15$	$\psi < 75°$
1	88.27	83.16
2,3,4	75.33	71.93
5,6,7	62.26	70.76
8	52.15	71.86
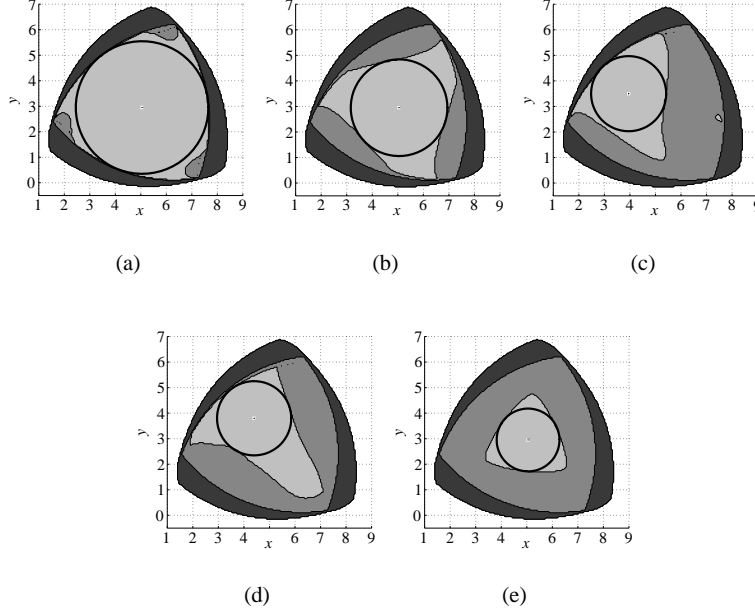
Fig. 3 RDW obtained with $\kappa_F^{-1}(\mathbf{J}) > 0.15$ of the (a) VAM; (b) 1st AM; (c) 2nd, 3rd and 4th AM; (d) 5th, 6th and 7th AM; (e) 8th AM

static performance of the VAM and its AMs within the workspace based on $\kappa_F^{-1}(\mathbf{J})$ (ψ, resp.). The dark zones depict the positions of P, in which ϕ cannot vary continuously between $5°$ and $25°$. The dark gray zones depict the positions of P, in which ϕ can vary continuously between $5°$ and $25°$, but $\kappa_F^{-1}(\mathbf{J})$ (ψ, resp.) is not necessarily higher (smaller, resp.) than 0.15 ($75°$, resp.). The light gray zones depict the positions of P, in which ϕ can vary continuously between $5°$ and $25°$ and $\kappa_F^{-1}(\mathbf{J})$ (ψ, resp.) is higher (smaller, resp.) than 0.15 ($75°$, resp.). Finally, the circles describe the RDW of the VAM and its AMs based on $\kappa^{-1}(\mathbf{J})$ (ψ, resp.).

Table 4 gives RDW radius of the VAM and its AMs obtained with $\kappa_F^{-1}(\mathbf{J}) > 0.15$ and $\psi < 75°$. We can notice that the results obtained with the two kinetostatic per-

formance indices are similar. Besides, the largest RDW is obtained with the 1st AM and the smallest one with 8th AM.

(a)   (b)   (c)

(d)   (e)
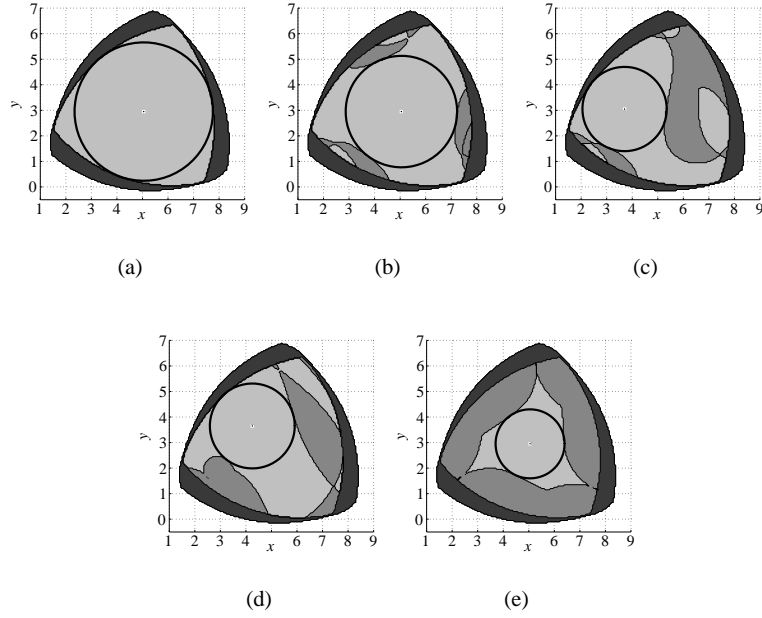
Fig. 4 RDW obtained with $\psi < 75°$ of the (a) VAM; (b) 1st AM; (c) 2nd, 3rd and 4th AM; (d) 5th, 6th and 7th AM; (e) 8th AM

Table 4 RDW radius of the VAM and its AMs obtained with the two kinetostatic performance indices

Actuating mode number	RDW radius	
	$\kappa_F^{-1}(\mathbf{J}) > 0.15$	$\psi < 75°$
1	1.89	2.18
2,3,4	1.47	1.65
5,6,7	1.45	1.66
8	1.23	1.35
VAM	2.60	2.71

4 Conclusions

In this paper, we introduced a new planar parallel mechanism with variable actuation, which is derived from the architecture of the 3-$\underline{R}$RR and 3-R$\underline{R}$R PPMs. Then, we used two indices, namely, the condition number of its kinematic Jacobian matrix and its transmission angle to compare its actuating modes. The concept of regular dextrous workspace was also used. It turns out that the mechanism with variable actuation can cover almost all its workspace with good and homogeneous kinetostatic performance as it takes advantage of the best performance of its actuating modes. Finally, for the mechanism at hand, we introduced equivalent bounds for the condition number and the transmission angle, which allow us to conclude that the two indices give similar results.

References

1. Alba-Gomez, O., Wenger, P. and Pamanes, A. (2005), Consistent Kinetostatic Indices for Planar 3-DOF Parallel Manipulators, Application to the Optimal Kinematic Inversion, *Proceedings of the ASME 2005 IDETC/CIE Conference*.
2. Arakelian, V., Briot, S. and Glazunov, V. (2007). Increase of Singularity-Free Zones in the Workspace of Parallel Manipulators Using Mechanisms of Variable Structure. *Mech. Mach. Theory*, Available online at www.sciencedirect.com.
3. Balli, S., and Chand, S. (2002), Transmission angle in mechanisms *Mechanism and Machine Theory*, vol. 37, no. 2, pp. 175–195.
4. Chablat, D. and Wenger, P. (1998), Working Modes and Aspects in Fully-Parallel Manipulator, *Proceeding IEEE International Conference on Robotics and Automation*, pp. 1964–1969, May.
5. Chablat, D., Wenger, P., Caro, S. and Angeles, J. (2002), The Isoconditioning Loci of Planar Three-DOF Parallel Manipulators, *Proc. DETC ASME*, Montreal, Canada.
6. Chablat, D., Wenger, P., Majou, F. and Merlet, J.P. (2004), An Interval Analysis Based Study for the Design and the Comparison of 3-DOF Parallel Kinematic Machines, *International Journal of Robotics Research*, vol. 23, no. 6, pp. 615–624.
7. Chablat, D. and Wenger, P. (2004), The Kinematic Analysis of a Symmetrical Three-Degree-of-Freedom Planar Parallel Manipulator," *CISM-IFToMM Symposium on Robot Design, Dynamics and Control*, Montreal.
8. Chen, C., and Angeles, J. (2005), A generalized transmission index for spatial linkages, *Proceedings of the ASME 2005 IDETC/CIE Conference*.
9. Golub, G. H. and Van Loan, C. F. (1989), *Matrix Computations*, The Johns Hopkins University Press, Baltimore.
10. Gosselin, C and Angeles, J. (1991), A Global Performance Index for the Kinematic Optimization of Robotic Manipulators, *ASME Journal of Mechanical Design*, vol. 113, pp. 220–226.
11. Li, Z. (1990), Geometrical Consideration of Robot Kinematics, *The International Journal of Robotics and Automation*, vol. 5, no. 3, pp. 139–145.
12. Merlet, J-P. (2006), *Parallel robots*, Springer.
13. Paden, B. and Sastry, S. (1988) Optimal Kinematic Design of 6R Manipulator, *The International Journal of Robotics Research*, vol. 7, no. 2, pp. 43–61.
14. Ranjbaran, F., Angeles, J., Gonzalez-Palacios, M. A. and Patel, R. V. (1995), The Mechanical Design of a Seven-Axes Manipulator with Kinematic Isotropy, *ASME Journal of Intelligent and Robotic Systems*, vol. 14, no. 1, pp. 21–41.

15. Theingin, Chen, I.-M., Angeles, J. and Li, C. (2007), Management of parallel-manipulator singularities using joint-coupling *Advanced Robotics*, vol. 21, no. 5-6, pp. 583–600.